A D-band high-gain antenna module combining an in-package active feed and a flat discrete lens

J L Gonzalez-Jimenez, F. Foglia Manzillo, A. Hamani, A. Siligaris, A. Clemente, C. Dehos

A D-Band High-Gain Antenna Module Combining an In-Package Active Feed and a Flat Discrete Lens

J. L. Gonzalez-Jimenez, F. Foglia Manzillo, A. Hamani, A. Siligaris, A. Clemente, C. Dehos

Univ. Grenoble Alpes, CEA, Leti, France

{joseluis.gonzalezjimenez, francesco.fogliamanzillo}@cea.fr

***Abstract* — This paper presents the design and experimental characterization of a high-gain D-band antenna module for high-capacity short-range links. The system comprises an active feed and a flat discrete lens. The active feed integrates a 45-nm CMOS two-channel transmitter, a diplexer and a four-element patch array on a low-cost laminate. This antenna-in-package excites a 48×48 planar lens which is designed using 16 different unit-cells and is optimized to collimate a broadside beam. The module operates over an 11.6% fractional bandwidth, between 139.4 GHz and 156.6 GHz, and delivers a peak effective isotropic power of 17 dBm.**

***Keywords* — CMOS, millimeter-wave circuits, millimeter-wave antennas, antennas-in-package, transmitarray antennas, active antennas.**

I. Introduction

Highly efficient D-band wireless systems could enable short-range links achieving unprecedented data rates. Novel broadband transmitter (TX) architectures are necessary to fully exploit the wide spectrum available in this band. The high propagation losses at these frequencies require the use of very high-gain antennas to maximize the link range. Moreover, energy efficiency is key to make such systems sustainable and attractive for mass production and for their deployment in next-generation wireless networks. Phased array antennas [1] leverage on multiple phase-shifted TX chains carrying copies of the same modulated signal to increase the effective isotropic radiated power (EIRP). Thus, high-directivity phased arrays, which comprise a large number of elements, exhibit a low radiation efficiency and a significant power consumption. Moreover, they often cover only narrow fractional bandwidths, e.g. 8.5% in [1]. A different approach to implement high-gain antennas for point-to-point links is presented in this work. The proposed architecture combines an active antenna feed, including an energy-efficient channel-bonding TX, similar to that in [2], and a planar lens. Both the lens and its feed are realized using low-cost printed circuit board (PCB) technology. The proposed solution achieves a bandwidth wider than that of state-of-the phased arrays of printed elements [1] and is based on a cheaper technology. It is more compact and versatile than quasi-optical systems based on shaped dielectric lenses [3].

II. Antenna Module Description

The active feed is an antenna-in-package (AiP) with a flip-chipped TX integrated circuit (IC). It is shown, along with its stack-up, in Fig. 1. The whole antenna system, with the flat lens excited by the active feed, is shown in Fig. 2. Both the lens and the AiP were fabricated using Isola Astra substrates ($\varepsilon_r = 3.0$ and $\tan\delta = 0.0017$) and a process resolution of 75 µm.

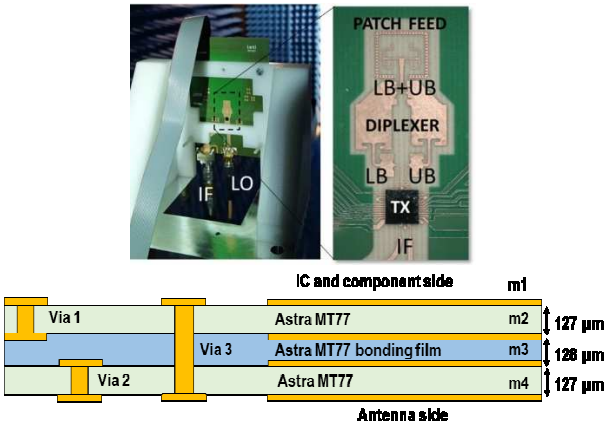

Fig. 1. Photographs and main sub-blocks of the AiP used as feed for the flat lens. Details of the flip-chipped TX IC, diplexer and microstrip feed of the patch array (top) and stack-up of the AiP (bottom).

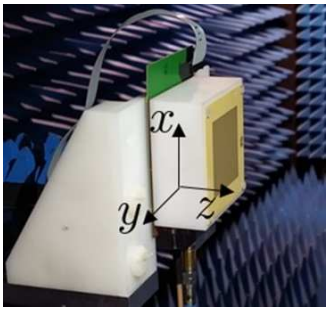

Fig. 2. Antenna module under test: the flat lens is spaced 30 mm apart from the AiP feed.

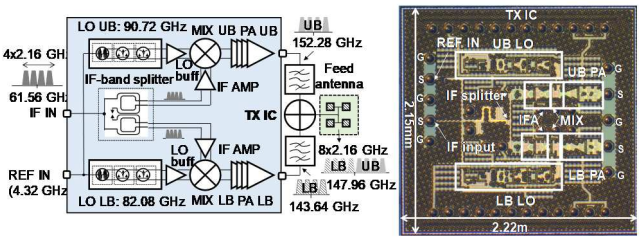

Fig. 3. Block diagram of the AiP and TX IC photograph.

The TX IC was fabricated in 45-nm CMOS radio-frequency silicon-on-insulator (RFSOI) technology. A block diagram and

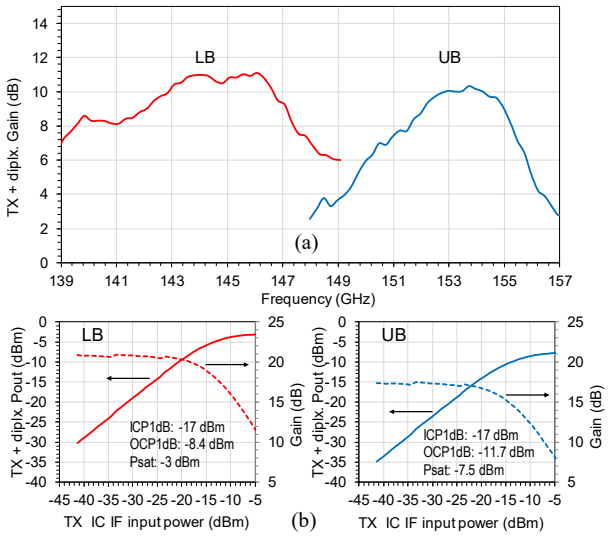

Fig. 4. (a) Measured gain as a function of the output frequency, and (b) output power and gain as a function of the IC IF input power for the sub-system comprising TX IC + diplexer.

a picture of the IC are shown in Fig. 3. The IC has two separate TX chains. Each chain delivers a modulated signal. The two IC output signals are centered at two different carrier frequencies. The two output signals of the IC cover two adjacent sub-bands around 148 GHz. They are recombined off-chip, using a substrate integrated waveguide (SIW) diplexer in the AiP (see Fig. 1 and Fig. 3). The output of the diplexer excites a patch array. Thanks to the proposed channel-bonding architecture, a signal with a relatively large fractional bandwidth (12%) can be transmitted.

The main building blocks of the proposed antenna system are described in the following sub-sections.

A. TX IC and diplexer: design and characterization

The TX IC porotype presented in this work has a single IF input that is divided in two using an on-chip passive splitter. Hence, the same IF input signal is reused by the two up-conversion lanes: each one up converts its copy to a different sub-band (namely the lower band LB and the upper band UB) at D-band. It is worth observing that, in the final system realization, the TX IC would have two separate intermediate frequency (IF) inputs. The IF signal band spans from 58 to 66 GHz. Each IF signal copy is mixed with a distinct internal local oscillator (LO) signal, at 82.08 GHz for the LB and 90.72 GHz for the UB. By doing so, two radio-frequency (RF) signals with adjacent spectra, are obtained. The total bandwidth covered by these D-band signals ranges from 139.4 GHz to 156.6 GHz. The LO generators use an external common input reference frequency at 4.32 GHz, from which the 19th and 21st harmonics (82.08 GHz and 90.72 GHz, respectively) are obtained on-chip. Finally, each RF signal is amplified by a couple of dedicated power amplifiers centered at 143.64 GHz and 152.28 GHz, respectively. The LB and UB signals go out of the chip separately and are combined by an SIW diplexer on the PCB.

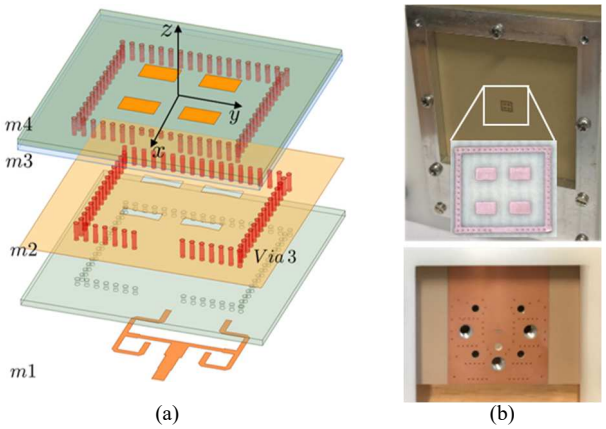

Fig. 5. (a) Structure of the 2×2 aperture-fed patch array of the active feed. (b) Stand-alone passive patch array prototype fed by an input waveguide-to-SIW transition on *m1* (see bottom inset).

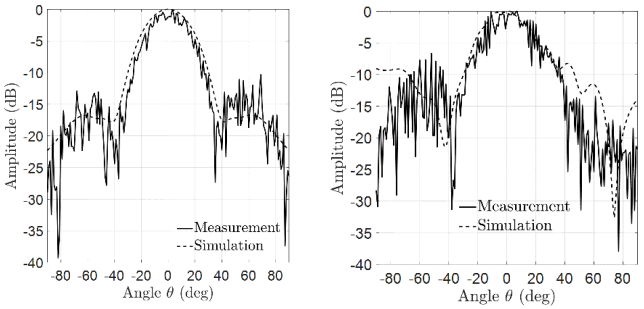

Fig. 6. Experimental and simulated patterns at 154 GHz of the stand-alone patch array prototype shown in Fig. 5b: (a) *yz*-plane and (b) *xz*-plane cut.

The resulting signal at the output of the diplexer is centered at 147.96 GHz and spans over a 17.28 GHz bandwidth.

The diplexer is realized on a double-sided 0.127-µm-thick substrate, between the metal layers *m1* and *m2* (see Fig. 1). The minimum via-diameter and conductor spacing are 80 µm. First, a stand-alone prototype was fabricated and characterized. The measured average insertion loss (IL) is about 8 dB at LB and 11 dB at UB [4]. A board in which the patch array antenna is replaced by a microstrip-to-WR6.5 transition was realized for characterizing the signal provided by the cascade of the TX IC and diplexer. More details on this testing board are presented in [2]. A continuous wave excitation was provided at the IF input of the board and power measurements were performed at the waveguide output. The measured gain of the sub-system comprising TX IC and diplexer is plotted in Fig. 4 (top), as a function of frequency. These results were obtained subtracting the IL of the input lines and output transition. The peak gain values are 12 dB and 10 dB, at the LB and UB, respectively. At the diplexer output, the peak power values at the 1-dB compression point are -8.4 dBm (LB) and -11.7 dBm (UB), as shown in Fig. 4 (bottom).

B. Patch antenna array: design and characterization

The recombined signal at the output of the diplexer excites a parallel-fed aperture-coupled 2×2 patch array. Such a small array is suitable for feeding high-gain lens antennas at relatively short distances [5]. The stack-up of the antenna is shown in Fig.

5a. The patches on *m4* (see Fig. 1) are evenly spaced 1.25 mm (0.67 λ_h) apart along both axes, where λ_h is the free-space wavelength at 160 GHz. The coupling slots, on *m2*, are excited by a 1-to-4 microstrip corporate feed on *m1*. Their lengths and widths are 0.80 mm and 0.18 mm, respectively.

The choice of the thicknesses of the substrates between *m2* and *m4* was made to prevent the propagation of higher-order grounded-slab surface-wave modes up to 208 GHz [6]. A 3.3mm×2.9mm cavity was designed around the array, using through-hole (*via3*) to hinder the propagation of the fundamental TM_0 surface-wave mode [3], [7], inherently supported by the grounded dielectric slab between *m2* and *m4*. A small aperture was realized in the cavity, around the input microstrip line.

The overall design was optimized using a commercial finite element solver, using the actual size of the AiP for the ground and substrates.The simulated input reflection coefficient is less than -10 dB between 130 GHz and 160 GHz, corresponding to a relative bandwidth of 20.7%.

A passive prototype (see Fig. 5b) was fabricated to evaluate the stand-alone performance of the array. The prototype is fed by a standard WR6.5 rectangular waveguide. A waveguide-to-SIW-to-microstrip transition, similar to that presented in [2], excites the microstrip corporate feed of the array on *m1*. Figure 5b shows a detail of the transition on *m1* and the mechanical support used to assemble the input waveguide on the board.

The far-field radiation pattern was measured in anechoic chamber. The prototype and the reference antenna were at a distance of 3 m. Measured and simulated patterns at 154 GHz are compared in Fig. 6a (H-plane cut) and Fig. 6b (E-plane cut). The E-plane pattern asymmetry is partly due to the input feed. The boresight realized gain of the antenna is obtained by de-embedding the scattering parameters of the input transition, which were characterized using a set of thru, reflect and line fixtures. It ranges between 8.7 dBi and 10.7 dBi in the 130–156-GHz band.

C. Flat Discrete Lens Design and Characterization

The flat lens is designed using 16 different phase-shifting unit-cells (UCs). All UCs have the same stack-up. They are via-less and comprise only three metal layers, interleaved by two dielectric substrates and a bonding layer, as illustrated in Fig. 7a. Two orthogonal wire-grid polarizers are designed on top and bottom metal layers. The width and edge-to-edge spacing of the strips are 0.13 mm and 0.245 mm, respectively, for all UCs. A polarization-rotating element is realized on the inner layer. It is optimized to rotate by 90° the incident field, introduce a desired phase shift on it and maximize the amplitude of the transmission coefficient [8]. Several different rotators, e.g. split ring resonator, H- and I-shaped elements, were designed to obtain a set of 16 UCs with transmission coefficient phases uniformly distributed in the 360° range at 140 GHz. Thus, the UCs enable a 4-bit quantization of the optimal flat lens aperture distribution at 140 GHz. The simulated transmission phases of the UCs under normal incidence using periodic boundary conditions are plotted in Fig. 7b. Between 125 GHz and 160 GHz, the maximum relative phase error is about 5° and the average insertion loss is about 0.4 dB, with a maximum value of 0.8 dB.

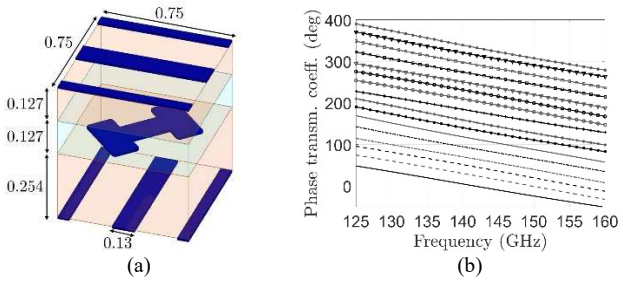

(a) (b)

Fig.7. (a) Stack-up of the UCs of the flat lens. A UC with I-shaped rotator is shown. Dimensions are in mm. (b) Phase of the transmission coefficients of the 16 UCs, simulated under normal incidence.

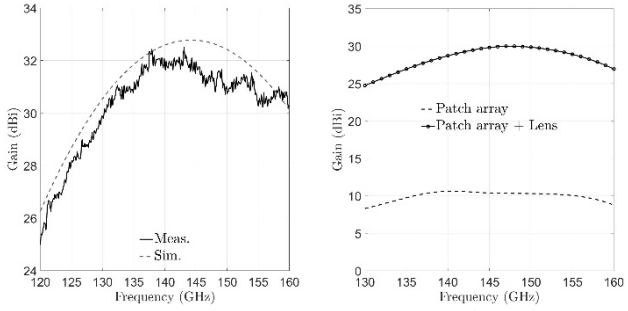

(a) (b)

Fig. 8. (a) Measured and simulated gain of a 48×48 broadside flat lens optimized for a 10-dBi horn feed at a distance of 25 mm. (b) Simulated broadside realized gain of the stand-alone patch array and of a 48×48 flat discrete lens illuminated by the same array, at a distance of 30 mm.

Moreover, the UCs have been miniaturized with respect to a similar 3-bit design at 300 GHz [8]. The edge of the proposed UCs is only 0.35λ_0, where λ_0 = 2 mm. The reduced UC size results in an enhanced performance under oblique incidence, as compared to standard designs with a period of 0.50 λ_0.

First, in order to validate the UC design and its technological feasibility, a square 2304-element lens was designed to collimate a beam at boresight at 148 GHz, using a 10-dBi gain horn as feed. The horn is aligned with the lens center and spaced 25 mm apart. The distribution of the UCs in the lens was optimized using a dedicated numerical tool [8]. The measured gain as a function of frequency follows the numerical results obtained using the tool, as shown in Fig. 8a.

Similarly, a broadside 48×48 discrete lens was then optimized to be illuminated by the AiP at a distance F = 30 mm. The simulated radiation pattern of the AiP were considered in the design. A 30-dBi gain at 148 GHz and a 3-dB gain bandwidth wider than the IC operating band (139.4-156.6 GHz) were targeted in the design. Figure 8b compares the computed broadside realized gain of the module and that of the AiP. A gain enhancement of about 20 dB is obtained using the lens.

III. Experimental Results

The complete antenna system (active feed and flat lens) has been characterized in an anechoic chamber. The input of the active feed is provided by a signal generator that delivers a single tone at the IF connector of the TX IC board. The IC generates a couple of D-band tones at the output at frequencies equal to the IF tone frequency plus the two internally generated

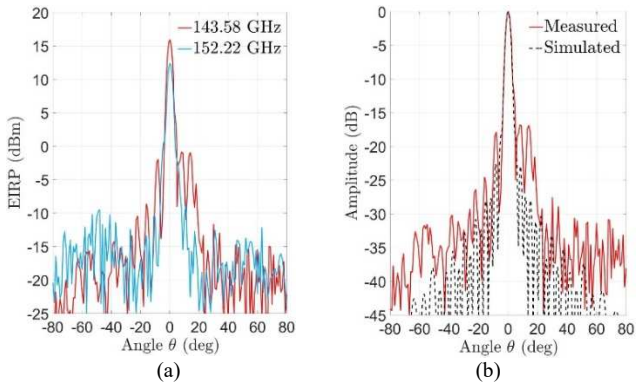

(a) (b)

Fig. 9. (a) Radiation patterns (*yz*-plane) of the antenna system for an input IF tone at 61.56 GHz. (a) Measured EIRP at 143.58 GHz and 150.20 GHz. (b) Simulated and measured normalized patterns at 143.58 GHz.

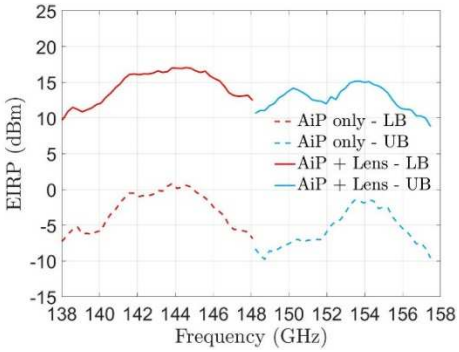

Fig. 10. Measured boresight EIRP at the 1-dB output compression point of the AiP for the stand-alone active feed and the overall antenna system.

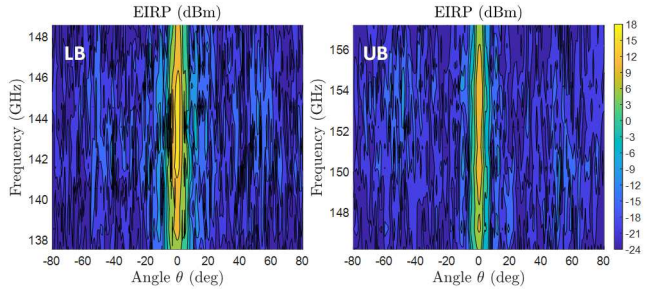

Fig. 11. Measured EIRP as a function of elevation angle (*yz*-plane) and frequency. The EIRP is measured at two different frequencies in the LB (left) and UB (right), both generated using a common input tone.

LO signals (82.08 GHz and 90.72 GHz). For example, when the IF signal is a 61.56 GHz tone, a tone at 143.64 GHz (LB) and another at 152.28 GHz (UB) are delivered at the two TX IC outputs, respectively. The SIW diplexer combines these two signals in a single output that feeds the antenna. By sweeping the IF signal frequency, the TX module sweeps simultaneously the two LB and UB bands. The emitted power is measured at 3.2 m using a 20-dBi standard gain horn and a spectrum analyzer with a D-band mixer extender. The received power is calibrated using the conversion gain table of the D-band mixer extender. The EIRP is measured at the 1-dB compression point of the TX IC. Figure 9a shows the EIRP, as a function of the elevation angle in the *yz*-plane (see Fig. 2), for an input IF tone at 61.56 GHz. The difference between the EIRP at the low and upper bands is mainly due to the frequency-dependent insertion loss of the SIW diplexer [2]. A similar gain drop, from LB to UB, was observed in the measured gain of the cascade of TX IC and diplexer (see Fig. 3). The comparison of measured and simulated radiation patterns (*yz*-plane) at 143.58 GHz is shown in Fig. 9b. A good agreement is observed. Some discrepancies can be seen for large angles. They are attributed to the simplified simulated feed model that comprises only the patch antenna. The EIRP at the boresight direction of the complete module (active feed + lens) is compared in Fig. 10 to that of the active feed, i.e. to the value measured without lens. The EIRP increase in the presence of the lens is between 17 and 19 dB in the entire band. These measured values are in agreement with the antenna gain increase predicted by the simulations in Fig. 8b. The EIRP and radiation patterns are stable versus frequency, in both sub-bands, as it can be observed from the contour plots presented in Fig. 11.

IV. Conclusion

In this work, a D-band high-directivity flat lens antenna excited by an AiP feed comprising channel-bonding TX has been demonstrated. The full module is realized using a low-cost PCB technology. It achieves a very competitive antenna gain (30 dBi) and fractional bandwidth of 12% centered at 148 GHz. The measured EIRP at the 1-dB compression point of the dual-channel TX IC is 17 dBm. These results are comparable to those achieved by other state-of-art systems that use more complex and power-consuming TXs, such as [1].

References

[1] S. Li, Z. Zhang, B. Rupakula and G. M. Rebeiz, "An Eight-Element 140 GHz Wafer-Scale Phased-Array Transmitter with 32 dBm Peak EIRP and > 16 Gbps 16QAM and 64QAM Operation," *IEEE MTT-S International Microwave Symposium (IMS)*, pp. 795-798, June 2021.

[2] A. Hamani, et al., "An 84.48 Gb/s CMOS D-band multi-channel TX system-in-package", *IEEE Radio Freq. Integr. Circ. Symp.*, Atlanta, USA, pp. 207-210, June 2021.

[3] A. Bisognin, et al., "Ball grid array module with integrated shaped lens for 5G backhaul/fronthaul communications in F-band", *IEEE Trans. Antennas Propag.*, vol. 65, no. 12, pp. 6380-6394, Dec. 2017.

[4] A. Hamani, et al., "Ultra-Broadband SIW Diplexer on Low-Cost Laminate Technology for Channel Bonding D-Band Front Ends" *51st European Microwave Conference (EuMC)*, pp. 433-436, April. 2022.

[5] F. Foglia Manzillo, *et al.*, "Low-cost, high-gain antenna module integrating a CMOS frequency multiplier driver for communications at D-band," in *Proc. IEEE Radio Freq. Integr. Circuits Symp. (RFIC)*, Boston, MA, USA, pp. 19-22, June 2019.

[6] C. A. Balanis, *Advanced Engineering Electromagnetics*, John Wiley & Sons, New York, 1989.

[7] A. Lamminen, J. Säily, J. Ala-Laurinaho, J. de Cos and V. Ermolov, "Patch antenna and antenna array on multilayer high-frequency PCB for D-Band," *IEEE Open J. Antennas Propag.*, vol. 1, pp. 396-403, 2020.

[8] O. Koutsos, F. Foglia Manzillo, A. Clemente, and R. Sauleau, "Analysis, rigorous design and characterization of a three-layer anisotropic transmitarray at 300 GHz," *IEEE Trans. Antennas Propag.*, early access, 2022.